Astronomy & Astrophysics manuscript no. aa
November 29, 2015

Multiply imaged QSOs in the Gaia survey

F. Finet[1,2] and J. Surdej[2]

[1] National Astronomical Observatory of Japan (NAOJ), 650 N. A'ohoku Place, Hilo, 96720 HI, USA
e-mail: finet@naoj.org
[2] Extragalactic Astrophysics and Space Observations (AEOS), Institut d'Astrophysique et de Géophysique, Liège University, Allée du 6 Août, 17 (Sart Tilman, Bât. B5c), 4000 Liège, Belgium

Received Month 00, Year; accepted Month 00, Year

ABSTRACT

Aims. We report a study on the statistical properties of the multiply imaged quasars to be detected within the Gaia survey.
Methods. Considering two types of potential deflectors, the Singular Isothermal Sphere (SIS) and the Singular Isothermal Ellipsoid (SIE), we estimate the number of multiply imaged quasars as well as the normalised distributions of the redshifts of the lensed sources and of their associated deflectors. We also investigate the distribution of the lensing events as a function of their angular size and apparent magnitude. We compare the Gaia survey for multiply imaged quasars to typical ground-based ones and to an ideal survey that would be carried out with a perfect instrument from space.
Results. Out of the 6.64×10^5 QSOs brighter than $G = 20$ to be detected by Gaia, we expect the discovery of about 2886 multiply imaged sources, 450 of these being produced by a late-type galaxy. We only expect ~ 1600 of these multiply imaged quasars to have an angular separation between their images large enough to be resolved from seeing limited observations, ~ 80 of them having more than 2 lensed images.

Key words. Gravitational lensing : strong – (galaxies:) quasars: general – (cosmology:) cosmological parameters

1. Introduction

The Gaia mission[1] is presently conducting an all sky coverage during 5 years. The satellite is equipped with 3 different instruments, namely an astrometric instrument, a radial velocity spectrometer and a photometric instrument. The latter produces two low resolution spectra in the blue and the red, from which the G_{BS} , G_{RS} and the global G-band magnitudes are derived (see Jordi et al. 2006, 2010 for the description of the photometric system). The survey is expected to be complete down to the G-band magnitude $G = 20$.

The main goal of the mission is to make a three dimensional map of our Galaxy, thanks to the measurement of the photometry, astrometry and proper motion of $\sim 10^9$ stars. Radial velocity measurements will be obtained for a sub-sample of brighter objects. The satellite is also expected to detect a very large number of extragalactic objects, among which QSOs. Detection of QSOs will be difficult at low galactic latitudes ($|b| < 25 - 30°$). Considering QSO detection in the remaining 60% of the sky, this should lead to the detection of $5.5 - 7 \times 10^5$ QSOs (Mignard 2012, Robin et al. 2012, Slezak 2007). This very large sample, in combination with the astrometry precision of the survey down to ~ 25 μ-as will lead to the direct construction of a new celestial reference frame in the optical, at least a hundred times denser than the ICRF, allowing to test general relativity (Mignard 2005). Among these sources, we expect the detection of multiply imaged QSOs due to gravitational lensing by foreground deflecting galaxies, which could be detected down to an angular separation of ~ 0.2" (Mignard 2012).

[1] http://sci.esa.int/gaia/

Imaging with Gaia is done by reconstruction of 2D-images from multiple 1D-drift scan images acquired in different directions (Harrison 2011). Due to the peculiar drift-scan imaging mode of Gaia, it is necessary to properly estimate the properties of the lensed population of QSOs in order to define a detection strategy for the lensing events. The statistical properties of the QSOs to be detected have been studied by Slezak (2007). In this paper we concentrate on the study of the expected statistical properties of the population of lensed QSOs. This information will be used to define the best strategy for the detection of these lensing events throughout the different scans generated by the satellite.

Because of the very large number of sources detected by Gaia, we expect the gravitational lenses to constitute an unprecedented large sample. Beside the scientific interest of each lensed source individually, these multiply imaged sources will constitute a statistical sample that may be used to constrain the cosmological mass density parameter Ω_m, through the statistics of gravitational lensing in the sample, as well as to study the evolution in the population of deflecting galaxies.

A previous rough estimation of the number of expected gravitational lenses in the Gaia mission has already been performed (Finet et al. 2012) and Mignard (2008) has studied the impact of gravitational lensing on the reference frame constituted by the sources. We here concentrate on the in-depth study of their expected statistical properties.

We introduce the mathematical formalism in the next section. We first derive an expression for the probability of a source to be lensed, alternatively modeling the deflectors by spherical (2.1.1) and elliptical (2.1.2) singular isothermal mass distributions. We then introduce in Section 2.2 the joint probability distribution of the Gaia QSOs in the redshift-absolute magnitude

plane that we use in the next subsections to calculate various expected distributions of astrophysical parameters linked to the lensed population. Specifically, the average lensing optical depth in the sample, the redshift distributions of the lensed sources and of the deflectors are derived. Finally, we derive an expression for the distributions of the lensed sources as a function of their apparent magnitude and the angular separation between the lensed images.

In Section 3, we present the observational data on which we base our simulations, we derive the best fit parameter for the QSO Luminosity function evolution models, based on the LF of Richards et al. (2006) and Palanque-Delabrouille et al. (2013), from which we infer the joint probability density of the sources for simulation purposes. Finally, in Section 4, we present the results of the simulations and study the impact of the cosmological mass density parameter Ω_m and that of the minimal angular separation resolvable in the survey. The latter is done by comparing the results for a perfect instrument, the Gaia observatory and typical ground-based surveys.

2. Mathematical formalism for gravitational lensing statistics

2.1. Lensing optical depth

Multiple images of a background source arise when a foreground galaxy is located close enough to the source line-of-sight. In the present work, the sources condisered are point-like QSOs. In order to calculate the probability for a source to be lensed due to the presence of a foreground deflector near its line-of-sight, it is therefore crucial to accurately model the volume density of the potential deflecting galaxies. The comoving volume density of deflectors with a line-of-sight velocity dispersion in the range σ to $\sigma + d\sigma$ is given by the Velocity Dispersion Function (VDF) $\Phi_\sigma(\sigma)$, which is modeled by the modified Schechter function (Sheth et al. 2003, Mitchell et al. 2005, Choi et al. 2007, Chae 2010)

$$\Phi_\sigma(\sigma)\, d\sigma = \Phi_* \frac{\beta}{\Gamma(\alpha/\beta)} \left(\frac{\sigma}{\sigma_*}\right)^\alpha \exp\left[-\left(\frac{\sigma}{\sigma_*}\right)^\beta\right] \frac{d\sigma}{\sigma}, \quad (1)$$

where Φ_* and σ_* are the characteristic volume density and line-of-sight velocity dispersion, α and β are the VDF slope at low and high σ and $\Gamma(x)$ is the complete gamma function.

Thanks to their larger mass, early-type galaxies are more efficient deflectors than late-type galaxies which tend to form lensed images with a smaller angular separation. The latter, although more numerous, were shown to constitute typically less than 10% of the lensing events in a flux limited sample from ground-based observations (Keeton et al. 1998, Kochanek et al. 2000). Nevertheless, the fraction of lensing events due to late-type galaxies increases with a better angular resolution of the survey (e.g. the CLASS survey where $\sim$ 25% of the lenses are due to spiral galaxies, cf. Browne et al. 2003). Therefore, thanks to the very good angular resolution of the Gaia survey, we expect late-type galaxies to contribute to a significant fraction of the lensed sources. In our simulations, we consider the population of deflectors to be formed by both early- and late-type galaxies.

Most of the lensing statistics study of the evolution with redshift of the deflector population are consistent with a no-evolution scenario or very small effect of the evolution (Chae 2010, Oguri et al. 2012). For our estimation we thus neglect the evolution effect in the deflector galaxy VDF and we use the value of the VDF parameters measured in the local universe by Choi et al. (2007), i.e. for early-type galaxies $\Phi_{*,E} = 8 \times 10^{-3}$ h^{3}Mpc^{-3}, $\sigma_{*,E} = 161$ km s^{-1} and $(\alpha_E, \beta_E) = (2.32, 2.67)$, and for late-type galaxies $\Phi_{*,L} = 66 \times 10^{-3}$ h^{3}Mpc^{-3}, $\sigma_{*,L} = 91.5$ km s^{-1} and $(\alpha_L, \beta_L) = (0.69, 2.10)$.

2.1.1. Singular Isothermal Sphere deflector

As a first approximation, the total mass distribution of early- and late-type galaxies is well modeled by means of the *Singular Isothermal Sphere* (SIS) profile, i.e. a spherically symmetric mass distribution with a volume density scaling as $\propto r^{-2}$, where r is the distance to the deflector center (see e.g. Koopmans et al. (2006) and Koopmans et al. (2009) for observational confirmation of the close to isothermal behaviour of the galaxy mass distribution). Such a deflector may lead to the formation of at most 2 lensed images of a background source, with an angular separation equal to twice the Einstein ring angular radius θ_E which is given by

$$\theta_E = \frac{4\pi\sigma^2}{c^2} \frac{D_{ds}}{D_{os}}, \quad (2)$$

where D_{ds} (respectively D_{os}) is the angular diameter distance between the deflector (respectively the observer) and the source and c is the speed of light.

A deflector located in the deflector plane (perpendicular to the source line-of-sight) at a redshift z_d will lead to the formation of multiple images of a source at redshift z_s with apparent magnitude m if it is located inside an area Σ_{SIS} called the lensing cross section centred on the projected source position, and defined by (Turner et al. 1984)

$$\Sigma_{SIS} = D_{od}^2 \theta_E^2 \iint_{S_y} B(m, \mathbf{y})\, d\mathbf{y}, \quad (3)$$

where D_{od} is the angular diameter distance between the observer o and the deflector d. We have introduced the coordinates $\mathbf{y} = (y_1, y_2)$, the projection on the deflector plane of the source position, normalised to the scale factor $D_{od}\theta_E$, i.e. the Einstein radius.

The *amplification bias* $B(m, \mathbf{y})$ is introduced to take into account the favourable bias in the calculation of the source lensing optical depth, arising because of the flux amplification in the lensing event, which leads for instance to the inclusion in flux limited samples, of sources intrinsically fainter. In our simulations, we estimate the amplification bias thanks to the source differential number counts function (DNCF) $n_m(m)$ as a function of their apparent magnitude m, thanks to the relation

$$B(m, \mathbf{y}) = \frac{n_m(m + 2.5 \log(A(\mathbf{y})))}{n_m(m)}, \quad (4)$$

where $A(\mathbf{y})$ is the total amplification of the lensing event, i.e the sum of the multiple image amplification moduli.

The integration area S_y in Eq. 3 represents the area (normalised to the scale factor) in which the presence of a deflector leads to the formation of a *lensing event*, defined as the detection of two lensed images by the survey strategy. Depending on the survey angular resolution, the associated 2-D integration interval S_y varies and so does the lensing cross section.

The probability $\tau_{SIS}(z_s, m)$ for a source with a redshift z_s and an apparent magnitude m to be multiply imaged, or the *lensing optical depth*, is obtained by integrating the density of deflectors (over all possible values of σ) located within the envelope of the

lensing cross sections at each intermediate redshift z, defined as the *lensing volume* (Nemiroff 1989). This leads to the expression

$$\tau_{SIS}\,(z_s, m) = \int_0^{z_s}\int_{\sigma_1}^{\sigma_2} (1+z)^3\,\Phi_\sigma\,(\sigma)\,\frac{cdt}{dz}\Sigma_{SIS}\,(z, z_s, m, \sigma)\,d\sigma\,dz, \tag{5}$$

where σ is in the range σ_1 to σ_2 associated with the deflector population and cdt/dz is the infinitesimal light-distance element, which in a flat FLRW universe is expressed as (Peebles 1993)

$$\frac{cdt}{dz_d} = \frac{c}{H_0\,(1+z_d)}\left[(1+z_d)^3\,\Omega_m + (1-\Omega_m)\right]^{-1/2}, \tag{6}$$

where Ω_m is the present-day value of the cosmological mass density parameter. The integration over σ in Eq. 5 may be performed analytically under the assumption of a non-evolving deflector population. Using Eqs. 2 and 3 , Σ_{SIS} may be expressed as

$$\Sigma_{SIS}\,(\sigma) = \left(\frac{\sigma}{\sigma_*}\right)^4 \Sigma_*, \tag{7}$$

where $\Sigma_* = \Sigma_{SIS}\,(\sigma_*, m)$. Inserting the latter expression into Eq. 5 and integrating over the σ range $[\sigma_1, \sigma_2[\mapsto [0, +\infty[$, it comes

$$\tau_{SIS}\,(z_s, m) = \beta\Phi_*\,\frac{\Gamma\left((\alpha+4)/\beta\right)}{\Gamma\,(\alpha/\beta)}\int_0^{z_s}(1+z)^3\,\frac{cdt}{dz}\Sigma_* dz. \tag{8}$$

2.1.2. Singular Isothermal Ellipsoid deflector

In order to reproduce lensing configurations with more than two lensed images, as observed among the known gravitational lens systems, a new model was introduced by Kormann et al. (1994): the *Singular Isothermal Ellipsoid* (SIE). This model introduces an internal ellipticity into the mass distribution, characterised by the *axis ratio q* between the axes of the projected mass distribution on the deflector plane. The SIE mass profile may produce 2, 3 (cusp configuration) or 4 lensed-images depending on the position of the source relatively to the caustics (defined as the lines of infinite amplification in the source plane). Non-singular mass profiles may produce an additional highly de-amplified central lensed-image, difficult to detect because very faint and dimmed by dust extinction in the deflector. Because this central lensed-image is not likely to be detected in the Gaia images, in the present work, we only consider the lensed-images produced by the SIE model and effectively detected on the CCD frames.

When considering an SIE deflector, the lensing cross section in Eq. 3 now depends on the deflector axis ratio. We may define a lensing event as the detection of multiple images, or as the detection of a given number i of lensed images (2, 3 or 4), accounting or not for the ability of the instrument to resolve lensed images with a too small angular separation. Consequently, depending on the definition of the lensing event, the area S_y in Eq. 3 varies and we therefore define different cross sections: Σ_{SIE} corresponds to the detection of multiple images irrespective of their number, and $\Sigma_{SIE,i}$ to the detection of i lensed images.

The volume density of the deflectors is now also a function of the axis ratio q. Due to the lack of observational constraints on the $q-\sigma$ correlation for the deflectors, we assume that the distribution of the axis ratio is independent of the deflector line-of-sight velocity dispersion. The number density of deflectors with a line-of-sight velocity dispersion and axis ratio in the range σ to $\sigma + d\sigma$ and q to $q + dq$, respectively, is thus

$$\Phi_\sigma\,(\sigma)\;n_q\,(q)\;d\sigma\,dq, \tag{9}$$

where $n_q\,(q)$ is the normalised distribution as a function of the axis ratio q for the case of early-type or late-type galaxies, and where the deflector VDF $\Phi_\sigma\,(\sigma)$ is given by Eq. 1.

Koopmans et al. (2006) and Sluse et al. (2012) have independently confirmed through the study of various gravitational lens samples that elliptical galaxy isophotes and the isodensity curves of their projected mass distribution have well correlated ellipticities and major axis directions. The normalised distribution $n_q\,(q)$ can thus be estimated from the distribution of the isophotes of early-type galaxies as measured by Choi et al. (2007) in the local universe.

To calculate the lensing optical depth $\tau_{SIE}\,(z_s, m)$ for a source with deflectors modeled by SIE mass profiles, we have to integrate over both variables σ and q (Huterer et al. 2005), which leads to

$$\tau_{SIE}\,(z_s, m) = \int_0^{z_s}\int_{\sigma_1}^{\sigma_2}\int_0^1 \left\{(1+z)^3\,\Phi_\sigma\,(\sigma)\,n_q\,(q)\,\frac{cdt}{dz}\Sigma_{SIE}\right\} dq\,d\sigma\,dz. \tag{10}$$

The integration over σ can be performed using Eq. 7 while adopting the same assumptions as for the SIS case. This leads to

$$\tau_{SIE}\,(z_s, m) = \beta\Phi_*\,\frac{\Gamma\left((\alpha+4)/\beta\right)}{\Gamma\,(\alpha/\beta)}\int_0^{z_s}(1+z)^3\,\frac{cdt}{dz}\int_0^1 \Sigma^*_{SIE}\,n_q\,(q)\,dq dz. \tag{11}$$

We have developed software toolboxes using *Matlab*, allowing us to calculate the lensing cross sections and optical depths, modeling the deflectors by means of both the SIS and the SIE mass distribution (Eqs. 3, 5 and 11)

2.2. The QSO joint probability density $d_{obs}\,(z_s, M)$

The sources detected in a survey are characterised by their absolute magnitude M and their redshift z_s. We can associate to each source a probability $P\,(z_s, M)$ to be detected with a redshift and an absolute magnitude in the ranges z_s to $z_s + dz_s$ and M to $M + dM$, respectively. Furthermore we may define the joint probability density $d_{obs}\,(z_s, M)$ associated to $P\,(z_s, M)$ by means of the relation

$$P\,(z_s, M) = d_{obs}\,(z_s, M)\,dz_s dM. \tag{12}$$

For an already existing survey, $d_{obs}\,(z_s, M)$ may be estimated from the normalised smoothed histogram in the (z_s, M) plane of the detected sources. However, for prospective simulation purposes, $d_{obs}\,(z_s, M)$ can be estimated by means of the QSO luminosity function $\Phi\,(z_s, M)$ (Oguri & Marshall 2010) by means of the relation

$$d_{obs}\,(z_s, M) = \frac{S\,(z_s, M)}{N_{QSO}}\,\Phi\,(z_s, M)\,\frac{dV_c}{dz}, \tag{13}$$

where

- $S(z_s, M)$ accounts for selection biases in the (z_s, M) plane, occurring during the detection procedure of the sources. For a perfect flux limited sample, this function equals one in the region of the (z_s, M) plane leading to an apparent magnitude brighter than the survey limiting magnitude.
- N_{QSO} is the total number of QSOs detected within the survey;
- dV_c/dz is the differential contribution at redshift z to the total comoving volume accessible by the survey, which in a flat expanding FLRW universe may be expressed as

$$\frac{dV_c}{dz} = D_c^2(z)\,\frac{dD_c}{dz}\,\Omega_{Gaia}, \tag{14}$$

where D_c is the line-of-sight comoving distance at redshift z, $\frac{dD_c}{dz}$ its differential contribution, and Ω_{Gaia} is the solid angle covered by the survey, in which QSO detection is possible.

The joint probability density $d_{obs}(z_z, M)$ is closely related to observable distributions of the source population. Indeed, the marginal distribution $n_z(z_s)$ obtained by integrating $d_{obs}(z_s, M)$ over M is the normalised redshift distribution of the sources. Similarly, the *differential number counts function* (DNCF) as a function of the apparent magnitude may be estimated by

$$n_m(m) = \frac{N_{QSO}}{\Omega_{Gaia}} \int_{z_1}^{z_2} d_{obs}(z_s, m - DM(z_s) - K(z_s))\,dz_s, \tag{15}$$

where $DM(z_s)$ and $K(z_s)$ are the distance modulus and K-correction at redshift z_s, respectively.

2.3. Source statistical properties

The joint probability density of the source population is directly linked to the distribution of the sources in the (z_s, M) plane, as well as to their observable distributions n_z and n_m. It may be used as a weighing factor to estimate the mathematical expectation of any function of z_s and M.

Let us assume that we have an expression for the lensing optical depth $\tau(z_s, M)$ as a function of z_s and M for a given source. This expression is trivially obtained from $\tau_{SIS}(z_s, m)$, $\tau_{SIE}(z_s, m)$ and $\tau_{SIE,i}(z_s, m)$ (Eqs. 5 and 11) considering $m = M + DM(z_s) + K(z_s)$. Its mathematical expectation $\langle\tau\rangle$ is simply given by

$$\langle\tau\rangle = \int_{M_1}^{M_2}\int_{z_1}^{z_2} d_{obs}(z_s, M)\,\tau(z_s, M)\,dz_s dM, \tag{16}$$

where $\langle\tau\rangle$ represents the fraction of sources in the detected population to have undergone a gravitational lensing event.

Similarly, the expected normalised redshift distribution of the deflectors $w_{z_d}(z_d)$ is given by (Oguri et al. (2012))

$$w_{z_d}(z_d) = \frac{1}{\langle\tau\rangle}\int_{M_1}^{M_2}\int_{z_1}^{z_2}\frac{d\tau}{dz}(z_s, z_d, M)\,d_{obs}(z_s, M)\,dz_s dM, \tag{17}$$

and the expected normalised redshift distribution of the lensed sources by (Oguri & Marshall 2010)

$$w_{z_s}(z_s) = \frac{1}{\langle\tau\rangle}\int \tau(z_s, M)\,d_{obs}(z_s, M)\,dM. \tag{18}$$

Integrating over the source redshift, we may also derive the normalised distribution $\omega_m(m)$ as a function of the apparent magnitude m of the lensed sources

$$\omega_m(m) = \frac{1}{\langle\tau\rangle}\int_{z_1}^{z_2}\tau(z_s, m - DM - K)\,d_{obs}(z_s, m - DM - K)\,dz_s. \tag{19}$$

Finally, let us define the normalised probability density ω_{θ_E} of observing a gravitational lens system with an angular configuration θ_E in the lensed population. From the definition of θ_E in Eq. 2, we may trivially derive the following relations

$$\frac{\theta_E}{\theta_*} = \left(\frac{\sigma}{\sigma_*}\right)^2 \Rightarrow \frac{1}{2}\frac{d\theta_E}{\theta_E} = \frac{d\sigma}{\sigma}, \tag{20}$$

where $\theta_* = \theta_E(\sigma_*)$. Furthermore, thanks to the definition of the lensing cross section in Eq. 3, we have

$$\Sigma_{SIS}(\theta_E) = \left(\frac{\theta_E}{\theta_*}\right)^2\Sigma_* \tag{21}$$

where $\Sigma_* = \Sigma_{SIS}(\theta_*)$ is the lensing cross section evaluated for the typical value of $\theta_E = \theta_*$. Inserting Eqs. 20 and 21 in the definition of τ_{SIS} in Eq. 5 and making use of Eq. 1, one may derive the expression of τ_{SIS} for which the integration is done over θ_E rather than σ. Deriving this expression with respect to θ_E, we find

$$\frac{d\tau}{d\theta_E}(z_s, M) = \int_0^{z_s}(1+z)^3\,\frac{cdt}{dz}\,\frac{\Phi_*\beta\Sigma_*}{\Gamma(\alpha/\beta)}\left(\frac{\theta_E}{\theta_*}\right)^{\alpha/2+2}\frac{e^{-\left(\frac{\theta_E}{\theta_*}\right)^{\beta/2}}}{2\theta_E}dz. \tag{22}$$

The normalised probability density ω_{θ_E} is then simply obtained by averaging the previous expression over the detected population of sources

$$\omega_{\theta_E}(\theta_E) = \frac{1}{\langle\tau\rangle}\int_{z_1}^{z_2}\int_{M_1}^{M_2}\frac{d\tau}{d\theta_E}(\theta_E, z_s, M)\,d_{obs}(z_s, M)\,dM\,dz_s. \tag{23}$$

Using the joint probability density $d_{obs}(z_s, M)$ as a weighing factor to average quantities over the entire population of sources detected in the survey, we have derived expressions for the mean optical depth $\langle\tau\rangle$ (Eq. 16), and of the normalised redshift distributions expected for the deflectors ω_{z_d} (Eq. 17) and for the lensed sources ω_{z_s} (Eq. 18). We have also derived the normalised distributions ω as a function of the apparent magnitude m and Einstein angle θ_E of the lensed sources (Eqs. 19 and 23, respectively).

The fundamental quantity needed is the joint probability density $d_{obs}(z_s, M)$ corresponding to the expected Gaia survey sources, which we estimate in the next section.

3. Observational constraints

In this section, we describe the observational constraints used to estimate the joint probability density $d_{obs}(z_s, M)$ for the Gaia survey.

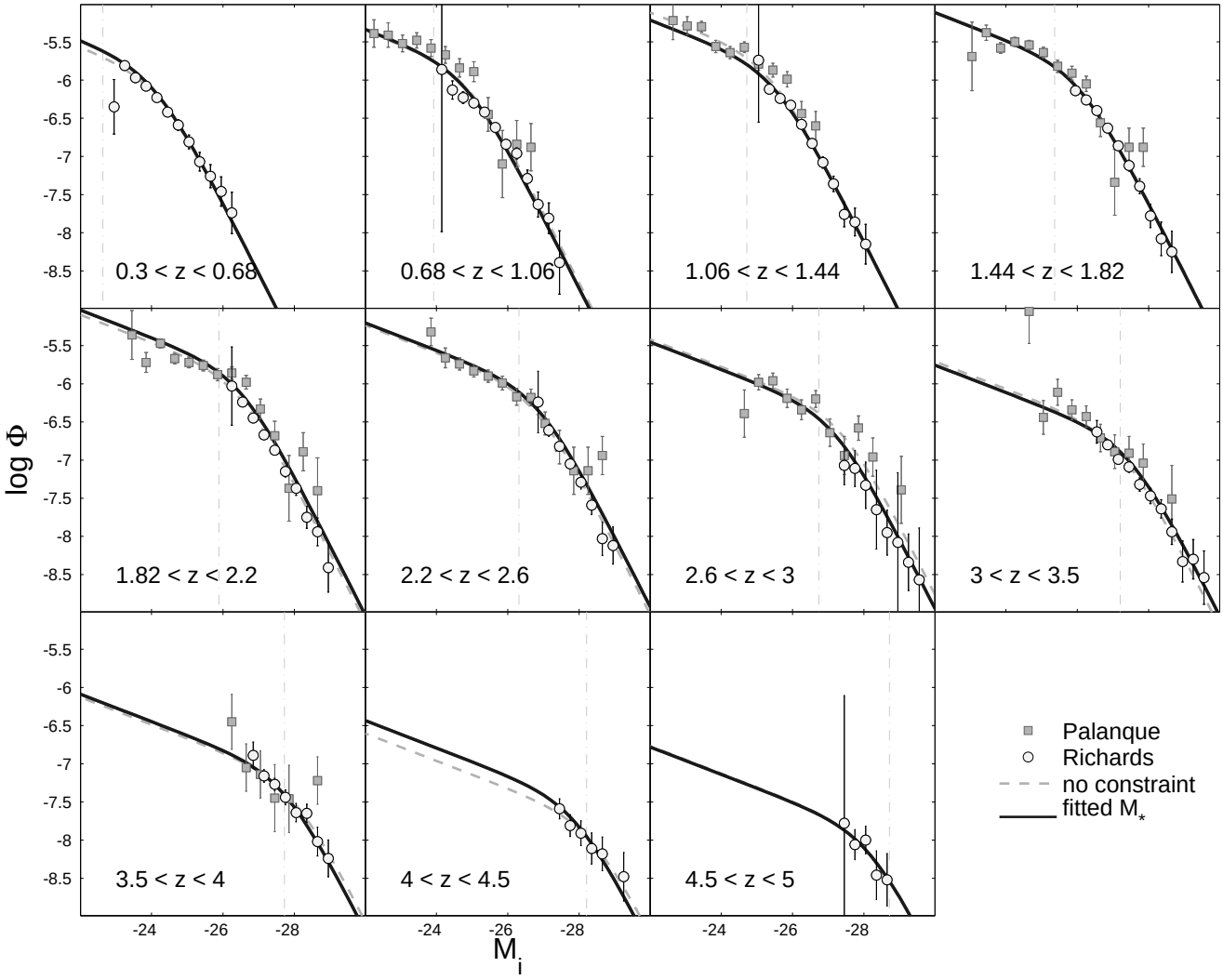

Fig. 1. Luminosity Function as a function of the absolute magnitude M_i in the SDSS i-band, for different redshift bins. We have included the LF determined by Richards et al. 2005 and Palanque-Delabrouille et al. 2013 (converted to M_i magnitude). The different fitted models correspond to : no contraints on the redshift behaviour of M_* and Φ_* (dashed light grey line); an evolution model for Φ_* and M_* is fitted freely (light grey line), M_* and Φ_* are both constrained by an evolution model (continuous black line). The latter is the final evolution model chosen for the simulations, see main text for the full description.

3.1. QSO luminosity function

Thanks to Eq. 13, $d_{obs}\,(z_s, M)$ may be estimated through the *Luminosity Function* (LF) of the observed sources. We need an estimate of the QSO Luminosity Function (LF) and its behaviour with redshift, spanning over the entire redshift and absolute magnitude ranges probed by the Gaia Survey. Various evolution models of the QSO optical LF have been proposed (e.g. Richards et al. (2005), Richards et al. (2006), Palanque-Delabrouille et al. (2013), Ross et al. (2012) for some recent works). Unfortunately, none of them fully spans over the entire redshift and absolute magnitude ranges accessed by the Gaia Survey.

In the remainder, we consider the binned luminosity function derived by Richards et al. (2006) as a function of the M_i magnitude (based on the SDSS-DR3) and that derived by Palanque-Delabrouille et al. (2013) in the SDSS g-band based on the SDSS-III and the MMT data, and we fit an evolution model on the combined data. Palanque-Delabrouille et al. (2013) have derived the binned LF versus the M_g continuum absolute magnitude associated with the SDSS g-band, with the zero point of the continuum K-correction at $z = 2$. For the conversion from M_g to M_i, we follow Ross et al. (2012) and convert through

$$M_i = M_g - 0.25. \tag{24}$$

This transformation is derived assuming the continuum to be a single power law with a spectral index $\alpha_\nu = -0.5$, which they have used for the definition of the continuum.

The derived binned luminosity function from Richards et al. (2006) and Palanque-Delabrouille et al. (2013) are depicted in Fig. 1, both expressed as a function of the M_i magnitudes, for the different redshift bins. Shen & Kelly (2012) have also derived the QSO LF from the SDSS-DR7, in the same redshift and apparent ranges as Richards et al. (2006) and their results are in very good agreement. We use Richards et al. (2006) because the redshift bins are similar to those of Palanque-Delabrouille et al. (2013).

We follow Richards et al. (2006) and we use absolute magnitudes M of the continuum, with a zero point of the continuum K-correction at redshift $z = 2$. We have determined the K-correction for the Gaia G-band using the G-band spectral transmission function (Jordi et al. 2010) with the QSO synthetic spec-

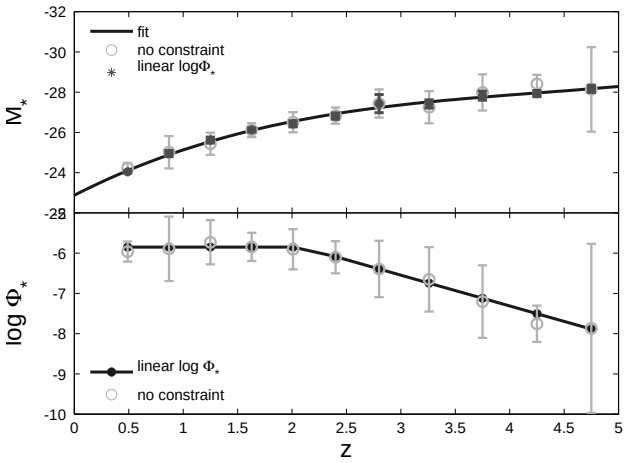

Fig. 2. Behaviour of the LF Φ_* and M_* parameters as a function of the QSO redshift. The dark continuous line shows the fit model used in our simulations. The light grey markers show the best fit parameters for Φ_* and M_* when fitting the LF separately in each redshift bin, without any evolution model constraints. When constraining the evolution of the characteristic density, the best parameters are found to be $\log \Phi_{*,lowz} = -5.85$, $\alpha_{\Phi_*} = -0.77 \pm 0.31$ and $z_{ref} = 2.09 \pm 0.28$.

trum derived by Vanden Berk et al. (2001), from SDSS QSO spectra. The definition of the continuum absolute magnitude and the derivation of the Gaia G-band K-correction are presented in Appendix A.

To facilitate the comparison with previous results, we determine the LF evolution considering absolute magnitudes M_i in the SDSS i-band. We convert the absolute magnitudes M_i to the Gaia G-band absolute magnitude M using the transformation law derived in Appendix A, based on the QSO spectrum from Vanden Berk et al. (2001), the G-band K-correction previously described and SDSS i-band K-correction given in Richards et al. (2006).

To model the LF, we use the conventional double power law form for the QSO LF in terms of absolute magnitudes

$$\Phi(z_s, M) = \Phi_* \left[10^{0.4(1+\alpha)(M-M_*)} + 10^{0.4(1+\beta)(M-M_*)} \right]^{-1}, \qquad (25)$$

where M_* and Φ_* are the characteristic absolute magnitude and number density, respectively. α and β are the bright and faint end slopes of the LF, respectively.

For the slope parameters, we consider $\beta = -1.45$ and $\alpha = -3.31$ (values taken from Richards et al. (2005) from the analysis of the combined SDSS and 2dF samples) over the entire redshift range.

We have first fitted the combined data in each redshift bin assuming constant slope parameters α and β, fitting Φ_* and M_* without any evolution model constraints on their behaviour as a function of the redshift. The resulting LF is shown as a dashed light-grey curve in Fig. 1 and the values of the best fit parameters are shown in Fig. 2 as light grey circles, for the different redshift bins. The rather large error bars arise because Φ_* and M_* are highly correlated.

Following the results of Ross et al. (2012), we assume that $\log \Phi_*$ is constant for $z < 2.05$ ($z < 2.2$ in Ross et al. 2012) and that it can be fitted as linearly evolving for higher z. We thus assume an evolution model for Φ_* given by

$$\begin{aligned} \log \Phi_* &= \log \Phi_{*,lowz} && , \text{if } z \leq z_{ref} \\ &= \log \Phi_{*,lowz} + \alpha_{\Phi_*} \left(z - z_{ref} \right) && , \text{if } z > z_{ref}. \end{aligned} \qquad (26)$$

In each redshift bin, for each Φ_* given by the model, we then fit the value of M_*. The best fit parameters are $\log \Phi_{*,lowz} = -5.85$, $\alpha_{\Phi_*} = -0.77 \pm 0.31$ and $z_{ref} = 2.09 \pm 0.28$.

The behaviour of Φ_* as a function of the redshift is shown in the lower panel of Fig. 2 and the corresponding fitted values of M_* are shown as dark grey markers on the upper panel.

Finally, motivated by the smooth redshift evolution of M_*, we fit the evolution of M_* by a third order polynomial. The fit is shown in the upper panel of Fig. 2. The best fit parameters are $[c_3, c_2, c_1, c_0] = [-0.0427, 0.5484, -2.7563, -22.8766]$.

The final evolution model used for M_* and $\log \Phi_*$ are shown as a function of the redshift, as a continuous dark grey line in Fig. 2. The corresponding LF is represented for the different redshift bins in Fig. 1, as a continuous dark grey line. We have represented for each redshift bin the faintest sources detectable by Gaia assuming $G = 20$ is the faintest magnitude achievable. The limit is shown as a vertical light-grey dashed-dotted line. The conversion from G to M_i is made using the colour $\langle G - i \rangle (z)$ evolution as a function of the redshift, described in Appendix A while adopting the SDSS i-band K-correction.

In the range accessible to the Gaia mission, our LF evolution model fits very well the data over the entire redshift range.

3.2. Joint probability density

In order to estimate the joint probability density $d_{obs}(z_s, M)$ for the Gaia survey, we use the QSO-LF function derived in Section 3.1 to compute $d_{obs}(z_s, M)$ through Eq. 13.

We limit the redshift range to $0 < z \lesssim 4.5$. Although the spectro-photometric imaging of Gaia will make possible to detect QSOs with a higher redshift, the limiting magnitude of $G = 20$ corresponds to very bright QSOs at redshift larger than $z \sim 4.5$ that are very rare.

The resulting $d_{obs}(z_s, M)$ is shown in the (z_s, M) plane on the left panel of Fig. 3. The grey scale is proportional to the probability of detection, a darker grey indicating a higher probability of detection. For clarity, we have indicated the magnitude cut-off of the survey $G = 20$ as well as the brighter cut-off $G = 16$, imposed because of the scarcity of such bright QSOs. For sources fainter than $G = 20$, d_{obs} is null as the detection probability of these sources is supposed to be null.

In order to assess the ability of the derived $d_{obs}(z_s, M)$ to reproduce the observed properties of the real sources, we compare the DNCF $n_m(m)$ as a function of the apparent magnitude thanks to Eq. 15, to observational sets that were used to determine the LF, by applying the magnitude and redshift cuts of the observational samples to the joint probability density.

Richards et al. (2006) have estimated the QSO DNCF in the SDSS i-band on the basis of the SDSS-DR3 QSO Catalogue, for sources restricted to the redshift ranges $0.3 < z < 2.2$ and $3 < z < 5$. In the lower redshift range, the survey is complete down to $i \simeq 19$. For the fainter magnitudes, we use the DNCF from the 2SQ/6QZ survey (also given in Richards et al. (2006)). The different data sets are displayed on the right panel of Fig. 3.

We have derived the DNCF from $d_{obs}(z_s, M)$ via Eq. 13, restricting the redshift range to $0.3 < z < 2.2$ and $3 < z < 5$. The results are shown on the right panel of Fig. 3, as the continuous and dashed light grey curves, respectively. The simulated DNCF are in very good agreement with the observational data. Following Richards et al. (2006), we use as definition of a QSO a source with an absolute magnitude in the continuum of the SDSS i-band (with zero point at $z = 0$) brighter than -22.5, considering a flat expanding universe with $H_0 = 70$ km s^{-1} Mpc^{-1} and $\Omega_m = 0.3$. On the same figure, we have represented as a dark grey line the

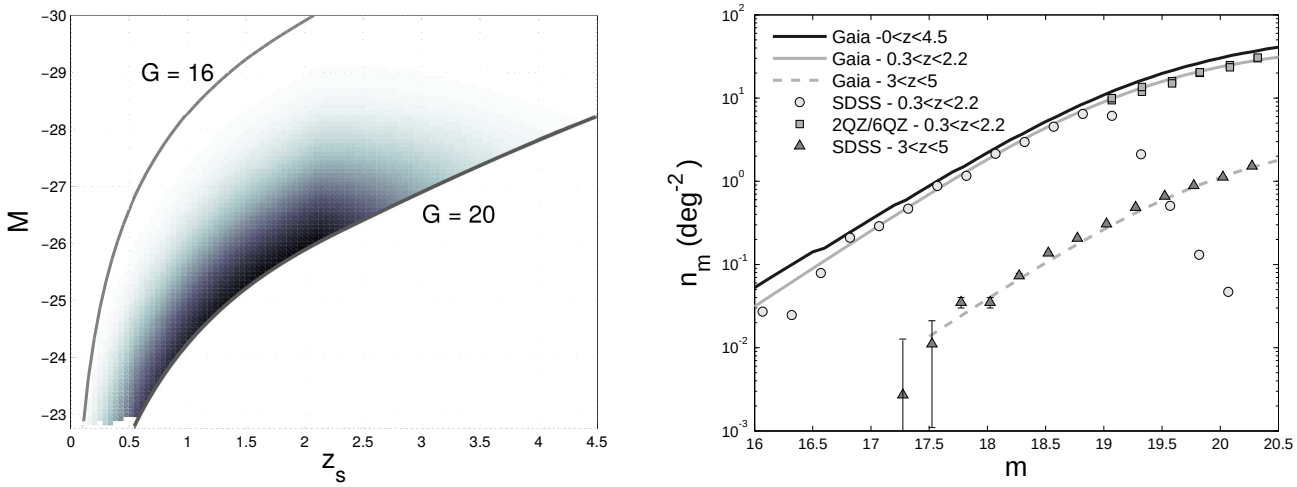

Fig. 3. Left: Joint probability density $d_{obs}\,(z_s, M)$ for the Gaia sources, derived using the LF evolution model described in the text. Right: DNCF as a function of the G-band magnitude. We use a combined observational sample of the SDSS-DR3 and 2QZ/6QZ for magnitudes brighter (respectively fainter) than $i \sim 19$, converted to G-band magnitudes and thus assuming the DNCF shape in G-band to be similar. We also show the fit used for the estimation of the DNCF.

Table 1. Comparison of the mean lensing optical depth and the expected number of detected multiply imaged quasars for different values of the survey angular resolution corresponding to a perfect survey (θ_{min} = 0"), Gaia (θ_{min} = 0.2") and typical ground-based observations (θ_{min} = 0.6"). For each value of θ_{min}, the table displays the average lensing optical depth $\langle\tau\rangle$ for both the SIS and SIE cases. In the latter case, the fraction of lensing events as a function of the number i of lensed images detected is also displayed $\langle\tau_i\rangle$ / $\langle\tau\rangle$. The bottom part of the table indicates the expected number of lenses in the survey, the total number as well as the number of events with a given number of detected lensed images. For comparison, we have reported the expected number of lensing events considering the population of sources found in Mignard 2012 and Slezak 2007, assuming that these sources have a similar distribution in the redshift-absolute magnitude diagram.

Survey	N_{QSO}	θ_{min} = 0"		θ_{min} = 0.2"		θ_{min} = 0.6"	
Early-type galaxies							
		SIS	SIE	SIS	SIE	SIS	SIE
$\langle\tau\rangle$	-	3.994×10^{-3}	3.747×10^{-3}	$\mathbf{3.917 \times 10^{-3}}$	$\mathbf{3.663 \times 10^{-3}}$	2.718×10^{-3}	2.431×10^{-3}
$\langle\tau_2\rangle$ / $\langle\tau\rangle$	-	-	0.917	-	0.92	-	0.948
$\langle\tau_3\rangle$ / $\langle\tau\rangle$	-	-	1.15×10^{-3}	-	2.564×10^{-2}	-	4.614×10^{-2}
$\langle\tau_4\rangle$ / $\langle\tau\rangle$	-	-	8.205×10^{-2}	-	5.25×10^{-2}	-	5.59×10^{-3}
This study	6.64465×10^5	2653	2490	**2602**	**2433**	1806	1615
3 images	-	-	3	-	62	-	75
4 images	-	-	204	-	134	-	9
Late-type galaxies							
		SIS	SIE	SIS	SIE	SIS	SIE
$\langle\tau\rangle$	-	1.278×10^{-3}	1.141×10^{-3}	$\mathbf{8.404 \times 10^{-4}}$	$\mathbf{6.815 \times 10^{-4}}$	-	-
$\langle\tau_2\rangle$ / $\langle\tau\rangle$	-	-	0.8413	-	0.92	-	-
$\langle\tau_3\rangle$ / $\langle\tau\rangle$	-	-	0.01206	-	0.07244	-	-
$\langle\tau_4\rangle$ / $\langle\tau\rangle$	-	-	0.1466	-	0.05192	-	-
This study	6.64465×10^5	849	758	**558**	**453**	-	-
3 images	-	-	9	-	33	-	-
4 images	-	-	111	-	24	-	-
All deflectors (early and late-type galaxies)							
		SIS	SIE	SIS	SIE	SIS	SIE
This study	6.64465×10^5	3502	3248	**3160**	**2886**	1806	1615
> 2 images	-	-	327	-	253	-	84
Mignard (2012)	$5.5 - 7 \times 10^5$						
Slezak (2007)	7.2×10^5						

expected DNCF $n_m\,(m)$ of the entire Gaia population, which is used in Eq. 4 when calculating the amplification bias.

Combining Eqs. 13 and 14, the normalisation factor of the joint probability density is Ω_{Gaia}/N_{QSO}, i.e. the number of QSOs detected per steradian, from which we may trivially derive the total number of QSOs expected to be detected in the survey. Considering that QSOs will be detectable over 60% of the sky (thus excluding the low galactic latitude fields), this leads to the expected detection of 6.64×10^5 sources, brighter than G = 20. Mignard (2012) has estimated the surface density of QSOs

brighter than $G = 20$ and concluded that the Gaia survey should expect the discovery of 5.5 to 7 $\times 10^5$ QSOs, a result in rather good agreement with our own estimate. Slezak (2007) also made a previous estimation of the number of QSOs to be detected: 7.2×10^5.

4. Results

We have computed the mean lensing optical depth $\langle\tau\rangle$ for the whole population of QSOs, by means of Eq. 16, for different values of the survey angular resolution θ_{min} (i.e. the *minimum* image separation for which point-like sources with similar amplification may be distinguished). In Eq. 16, we have alternatively considered the lensing optical depth τ for deflectors modeled as SIS (τ_{SIS} in Eq. 5) and as SIE deflectors (Eq. 11), considering the population of both early and late-type galaxies. When considering SIE deflectors, we have calculated both τ_{SIE} and $\tau_{SIE,i}$. In Fig. 4, we have represented, as a function of the angular resolution θ_{min} of the survey, the dependence of the different average optical depths $\langle\tau_{SIS}\rangle$, $\langle\tau_{SIE}\rangle$ and $\langle\tau_{SIE,i}\rangle$, as well as the evolution of the fraction of events with formation of 3 or 4 lensed images, i.e. $\langle\tau_{SIE,3}\rangle$ / $\langle\tau_{SIE}\rangle$ and $\langle\tau_{SIE,4}\rangle$ / $\langle\tau_{SIE}\rangle$, for both types of galaxy populations.

The average total optical depths $\langle\tau_{SIS}\rangle$ and $\langle\tau_{SIE}\rangle$ show a very similar behaviour: they both decrease as θ_{min} increases, as lensing events with images too close to each other are not resolved by the survey and are detected as single sources. In Table 1, we give the numerical values of the lensing optical depth for different values of the θ_{min} parameter, representative of a perfect survey ($\theta_{min} = 0$"), the Gaia survey ($\theta_{min} = 0.2$") and seeing-limited ground-based observations ($\theta_{min} = 0.6$"). θ_{min} represents the smallest angular separation between two point-like sources with similar brightness, for which the survey source detection procedure is capable to separate the two lensed images. We consider θ_{min} to be independent of the relative brightness between the lensed images. This assumption is motivated by the fact that the regions contributing the most to the lensing cross sections are the most amplified ones (where the source is located inside and near the tangential caustics). For these configurations, the brighter and closer lensed images are the ones located near the tangential critical curve and show similar amplification (see e.g. Schneider et al. 1992 , Ch. 6). In the case of typical ground-based observations, we consider seeing limited observations (typically $\sim 1 - 1.2$"). Thanks to PSF-fitting techniques, we may at best resolve point-like images with same brightness separated by half the PSF full width at half maximum, i.e. half of the seeing value.

For the early-type galaxy population, the average lensing optical depth for a perfect survey is 3.994×10^{-3} (3.747×10^{-3} for the SIE lens model) and is only a few percent lower in the case of the Gaia survey, i.e. 3.917×10^{-3} (3.663×10^{-3}). For the case of seeing-limited ground-based surveys however, about one third of the lensed sources are unresolved, with the mean lensing optical depth dropping to 2.718×10^{-3}(2.431×10^{-3}). Considering the estimated number of 6.64×10^5 sources to be detected by the Gaia survey, there are thus 2653 (2490) expected lensed sources, out of which 2602 (2433) should be detected by the Gaia survey. On the other hand, the seeing-limited ground-based follow up of the lensing events will only be possible for 1806 (1615) of them, unless adaptive optics observations will be made possible using large telescopes.

Considering now the late-type galaxy population, although more numerous, they are less efficient deflectors because of their lower mass. The average lensing optical depth for the Gaia survey is 0.84×10^{-3} (0.68×10^{-3} for the SIE lens model) but, because they tend to form lensing events with lensed-images closer to one another, they represent a negligeable fraction for typical seeing-limited ground-based observations. This deflector population should lead to the formation of 558 (respectively 453 for the SIE lens model) multiply-imaged quasars.

In conclusion, combining the expectation of the early- and late-type galaxy populations, the Gaia survey is expected to lead to the detection of 3160 (respectively 2886 for the SIE lens model) multiply imaged quasars.

These results are consistent with a former simplified estimation of the number of gravitational lens systems to be detected by Gaia in Finet et al. (2012), who found $\langle\tau\rangle = 5.9 \times 10^{-3}$, for the case of SIS deflectors and without taking into account the finite instrument resolution and considering only the population of early-type galaxies. The authors used a flat FLRW universe with $\Omega_m = 0.27$ and $H_0 = 72$ km s^{-1} Mpc^{-1}. Considering the same universe model and a perfect instrument, we find $\langle\tau_{SIS}\rangle = 4.3 \times 10^{-3}$. The slight differences are likely due to the fact that they considered sources as bright as $G = 15$ being affected by a larger amplification bias and a redshift range up to $z = 5$, thus slightly overestimating the very high redshift sources having a larger optical depth.

$\langle\tau_{SIS}\rangle$ and $\langle\tau_{SIE}\rangle$ lead to a very similar estimation of the number of lensed sources to be detected, and show a similar behaviour as a function of the angular resolution parameter θ_{min} as seen in Fig. 4. Nevertheless, the SIS model leads to a lensing optical depth estimate about 10% larger than that of the SIE model. This is due to the fact that the SIE mass distribution, initially introduced to conserve the projected mass inside iso-density curves with respect to the SIS case (Kormann et al. 1994), does not preserve the size of the geometrical cross section i.e. the area inside the caustics. For very elliptical deflectors, the geometrical cross section of the SIE deflector is smaller than that of the SIS, due to a flattening of the radial caustic curve when the ellipticity increases. Furthermore, the probability for a lensed source to have a given total amplification is different for the two mass distributions, thus leading to a different amplification bias effect (Huterer et al. 2005).

From Fig. 4, we see that among the gravitationally lensed sources, the configurations with 2 detected images are the most likely. Furthermore the fraction of events with 2 lensed images increases as θ_{min} increases, going from 91.7% for a perfect survey to 94.8% for $\theta_{min} = 0.6$" (cfr Table 1) for the early-type galaxy deflectors, because some configurations with 3 or 4 formed images have only 2 resolved images. We see a similar behaviour for the results considering the late-type deflectors. We have represented in Fig. 4 the evolution of the fraction of events with 3 or 4 detected lensed images as a function of θ_{min}. From Table 1, considering the early-type galaxy deflectors, we see that 204 lensed sources are expected to be composed of 4 lensed images (3 with 3 lensed images), but because of the limited angular resolution of the satellite, only 134 (respectively 62) are expected to be detected with 4 (respectively 3) observable lensed images. Out of these, 75 (respectively 9) lensing events with 3 (respectively 4) lensed images will be observable by means of seeing-limited ground-based observations, allowing to complement the times series and spectra acquired by the satellite. For what concerns the late-type population, they should lead to the formation of 57 events with more than 2 lensed-images among the lensed sources in the Gaia survey, none of which could be detected in a seeing-limited ground-based survey.

The lensed sources to be detected by the Gaia mission will thus constitute an unprecedented statistical sample, at least an order of magnitude larger than the existing ones, such as the

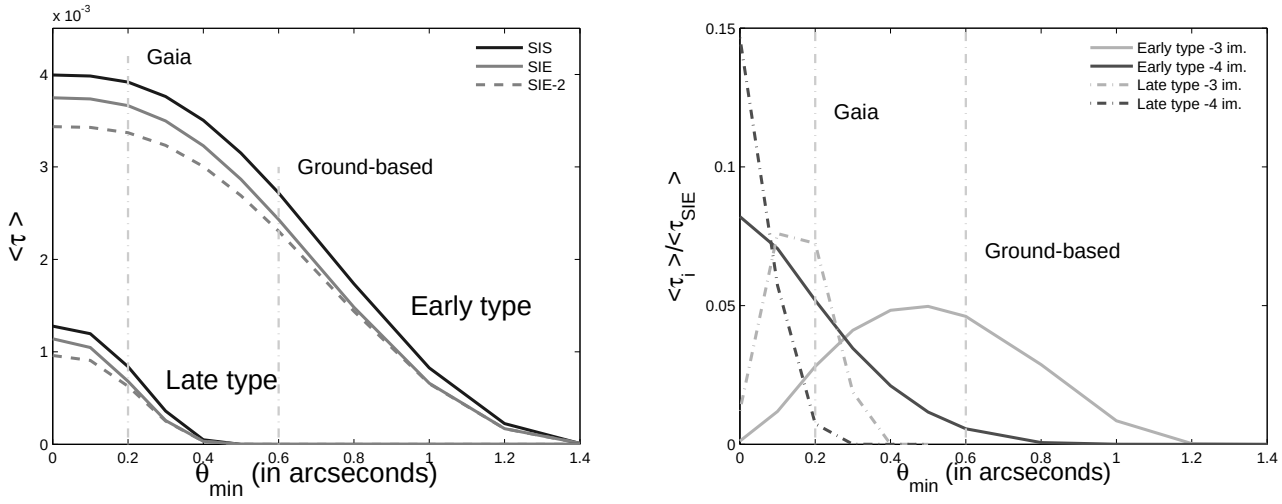

Fig. 4. *Left:* Average lensing optical depth as a function of the survey angular resolution θ_{min}, for the early- and late-type galaxy deflectors. We have modeled the deflectors as SIS ($\langle\tau_{SIS}\rangle$-continuous black line) and SIE mass distributions ($\langle\tau_{SIE}\rangle$-continuous gray line). In the latter case, we also show the average optical depth with detection of 2 lensed images ($\langle\tau_{SIE,2}\rangle$ - dashed gray line). *Right:* Fraction of lensed sources detected with 3 (light gray) or 4 (dark gray) lensed images, as a function of θ_{min}. The results for the case of early- and late-type galaxy deflectors are shown with continuous and dash-dotted lines, respectively. In both panels, we have indicated the typical value of θ_{min} for the Gaia survey and typical seeing limited ground-based observations.

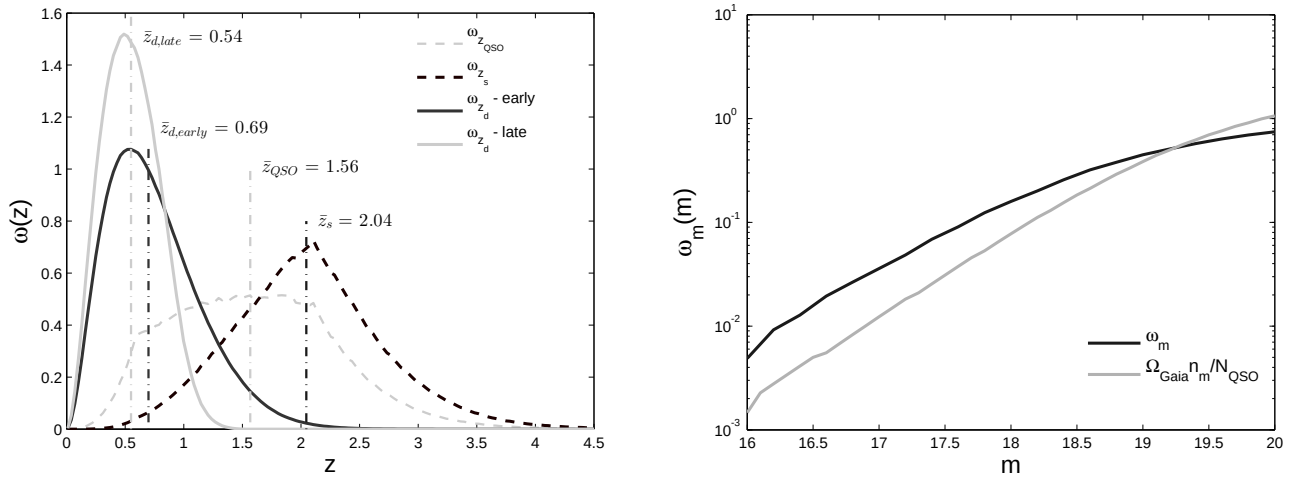

Fig. 5. *Left:* Expected normalised distributions ω as a function of the redshift of the lensed sources (z_s) and of the deflectors (z_d). For comparison, we have also included the normalised redshift distribution of the sources (ω_{QSO}). The simulations were done assuming θ_{min} = 0.2". We have indicated the median value of each distribution ($\bar{z}_s$, $\bar{z}_d$ and $\bar{z}_{QSO}$). *Right:* normalised distribution $\omega_m(m)$ of the lensed sources as a function of the apparent magnitude. For comparison, we show the DNCF as a function of the magnitude of all the detected sources, normalised by N_{QSO}/Ω_{Gaia}.

ground-based SDSS Quasar Lens Search sample (62 lensed sources, 26 in the statistical sample, see Inada et al. 2012) or the 13 lenses from the CLASS statistical sample (Browne et al. 2003).

On the left panel of Fig. 5, we show the expected normalised redshift distributions of the lensed sources $\omega_{z_s}(z)$ and of the deflectors $\omega_{z_d}(z)$. We have computed these distributions using Eqs. 17 and 18, assuming the typical angular resolution of Gaia θ_{min} = 0.2". For the normalised deflector redshift distribution, we have represented the expected distributions for the early- and the late-type deflector populations. For comparison, we have represented the normalised redshift distribution of the sources (ω_{QSO}), obtained by integrating $d_{obs}(z_s, M)$ over M. As the latter is a normalized joint distribution, its marginal distribution ω_{QSO} is normalized as well.

We have also indicated the median value of each distribution ($\bar{z}_s$, $\bar{z}_{d,early}$, $\bar{z}_{d,late}$ and $\bar{z}_{QSO}$). We clearly observe a shift for the lensed population towards higher redshifts compared to the entire population of QSOs, with a distribution shifting from $\bar{z}_{QSO}$ = 1.56 to $\bar{z}_s$ = 2.04. This is mainly explained by the increase of the geometrical lensing volume with the source redshift, which introduces a favourable bias towards sources located further away. The shape of ω_{z_s} is also influenced by the amplification bias which in our case favors low redshift sources. Indeed, as these sources have in average a brighter apparent magnitude (then those with a higher redshift), their amplification bias calculated through Eq. 4 is larger, thanks to the steeper slope of the DNCF for these magnitudes.

The normalised redshift distributions of the deflectors are different for the early- and the late-type ones. For a perfect instrument (i.e., θ_{min} = 0"), these distributions would be identi-

cal, as demonstrated in Appendix B. But in this simulation we have considered $\theta_{min} = 0.2$". This excludes lensing events with lensed-images having a too small image separation. Therefore, the fraction of rejected lensing events is higher for the late-type galaxy population. Furthermore, for a given source redshift, the first lensing events to be rejected are those with a higher deflector redshift (because the Einstein angular radius scales as $\theta_E(\sigma, z_d, z_s) \propto D_{ds}(z_d, z_s)/D_{os}(z_s)$). This leads to a normalised deflector redshift distribution peaking at lower redshift for the late-type galaxy population.

The normalised distributions as a function of redshift of the lensed sources $\omega_{z_s}(z)$ and of the deflectors $\omega_{z_d}(z)$ show no dependence with the deflector model chosen: both the SIS and SIE models lead to exactly the same distributions. Furthermore, the normalised redshift distribution of the lensed sources $\omega_{z_s}(z)$ is identical when considering the early or late-type galaxy populations.

On the right panel of Fig. 5, we have illustrated the normalised distribution $\omega_m(m)$ of the lensed sources as a function of their apparent magnitude, computed from Eq. 19 for the case of the SIS lens model. For comparison, we have shown the DNCF as a function of the magnitude of all the detected sources, normalised by N_{QSO}/Ω_{Gaia}, the number of sources detected per solid angle in the magnitude range $16 < m < 20$. We see that the distribution of the lensed sources presents an excess of brighter sources, benefiting from the amplification bias. In our simulations, we have found no effect of the angular resolution θ_{min} on $\omega_m(m)$. We have also found no differences between the ω_m distributions when considereing the early and late-type deflector populations.

Let us now analyse the impact of the finite instrumental resolution on these different distributions. As we have shown that modeling the deflectors by means of the SIE and SIS mass distributions leads to exactly the same normalised distributions $\omega_{z_s}(z)$ and $\omega_{z_d}(z)$, in order to minimize the computation time, we have only considered in the remainder the case of the SIS deflectors. On the left panel of Fig. 6, we display the normalised distribution of the deflectors $\omega_{z_d}(z)$ and its cumulative function, as a function of the deflector redshift, for three different values of the angular resolution θ_{min} corresponding to the perfect instrument case, the Gaia mission and typical ground-based observations.

The normalised and cumulative distributions corresponding to $\theta_{min} = 0$" and $\theta_{min} = 0.2$" look similar. When compared to the case of the ground-based observations ($\theta_{min} = 0.6$"), we conclude that the effect of the loss in resolution power is to miss the lensing events with a deflector at higher redshift. This may be easily understood for the SIS case. An SIS deflector produces 2 lensed images separated by an angle equal to twice the Einstein angle θ_E. From the definition of the Einstein angle in Eq. 2, θ_E scales as

$$\theta_E(\sigma, z_d, z_s) \propto \frac{D_{ds}(z_d, z_s)}{D_{os}(z_s)}. \quad (27)$$

For a source at a redshift z_s, $D_{ds}(z_d, z_s)$ is a decreasing function of the deflector redshift, consequently, θ_E decreases as the deflector redshift z_d increases, which will produce lensing events with images closer to each other, the first to be discarded as θ_{min} increases.

Let us now look at the cumulative distribution as a function of the redshift of the deflectors. For simplicity, we have only considered here the early-type galaxy population. In the case of the ground-based observations, 90% of the observed lensed sources have a deflector with a redshift smaller than $z = 0.88$. Most of the studies of the evolution effect in the deflector population based on lensing statistics are compatible with a no-evolution scenario or very little evolution of the deflectors (Oguri & Marshall (2010), Chae 2010 and Oguri et al. 2012). But ground-based observations (from which most of the statistical samples of lenses are issued) are very inefficient to study the evolution of the deflector population as they cut out all lens systems with a deflector at high redshift and are thus only suitable to study the low redshift population (typically, $z < 0.88$).

In the case of the Gaia mission, $\sim 30\%$ of the detected lenses due to the early-type galaxy population will have a deflector at a redshift larger than $z > 0.88$, i.e. ~ 800 lenses assuming the 2433 lenses to be detected, and ~ 240 lensed sources will have a deflector in the redshift range $1.27 < z_d < 2$. The statistical sample of lenses to be unravelled by the Gaia mission will thus provide a sample very well suited for the evolution study of the population of early- and late-type galaxies at high redshift, thanks to both the very large number of sources and the high angular resolution power for the detection of the lensed sources.

We have also computed the normalised distribution $\omega_{z_s}(z)$ of the lensed sources as a function of the redshift, for different values of θ_{min}. The angular resolution parameter θ_{min} has absolutely no impact on $\omega_{z_s}(z)$. This implies that the relative decrease in the lensing optical depth due to an increase in θ_{min} is independent of the source redshift and absolute magnitude. To understand this, we have computed the cumulative distribution of $d\tau/dz_d$, normalised to the source optical depth for the case of a perfect survey, i.e.

$$\frac{1}{\tau(z_s, m, \theta_{min} = 0")} \int_0^z \frac{d\tau}{dz_d}(z', z_s, m, \theta_{min})\, dz'. \quad (28)$$

The behaviour of the cumulative distribution in Eq. 28 as a function of the redshift is shown in Fig. 6. We show the case of two different sources at redshift $z_s = 2$ and 4, considering three different angular resolutions $\theta_{min} = 0, 0.6$ and 1", and modeling the deflector with both the SIS and SIE deflectors. For the clarity of the figure, we do not show the case for $\theta_{min} = 0.2$".

Let us first observe the case $\theta_{min} = 0$" (shown as a black dashed line). For this case, the normalised cumulative distributions are identical for the SIS and SIE cases. As the distributions corresponding to the different z_s differ, the differential contribution to the lensing optical depth is different for the two sources. Nevertheless, in the case of the $\theta_{min} = 0.6$" instrumental resolution, we observe that the fraction of the optical depth lost due to an increase in θ_{min} is the same for $z_s = 2$ and 4, for both the SIS and SIE cases. The fraction of the optical depth lost due to an increase in θ_{min} is thus independent on the redshift, or in other words, the ratio

$$\frac{\tau(z_s, m, \theta_{min})}{\tau(z_s, m, \theta_{min} = 0")} \quad (29)$$

is independent of the source redshift. We have computed the same distribution for sources having different apparent magnitudes and found no impact of the source magnitude on the distribution in Eq. 28.

As a consequence, the behaviour as a function of θ_{min} of the average optical depth $\langle\tau\rangle$ can be computed by considering the case of a perfect instrument, and calculating the ratio in Eq. 29 for a source with a random chosen redshift and magnitude.

4.1. Impact of Ω_m

On the left panel of Fig. 7, we show the evolution of the average lensing optical depth $\langle\tau\rangle$ as a function of the cosmological matter

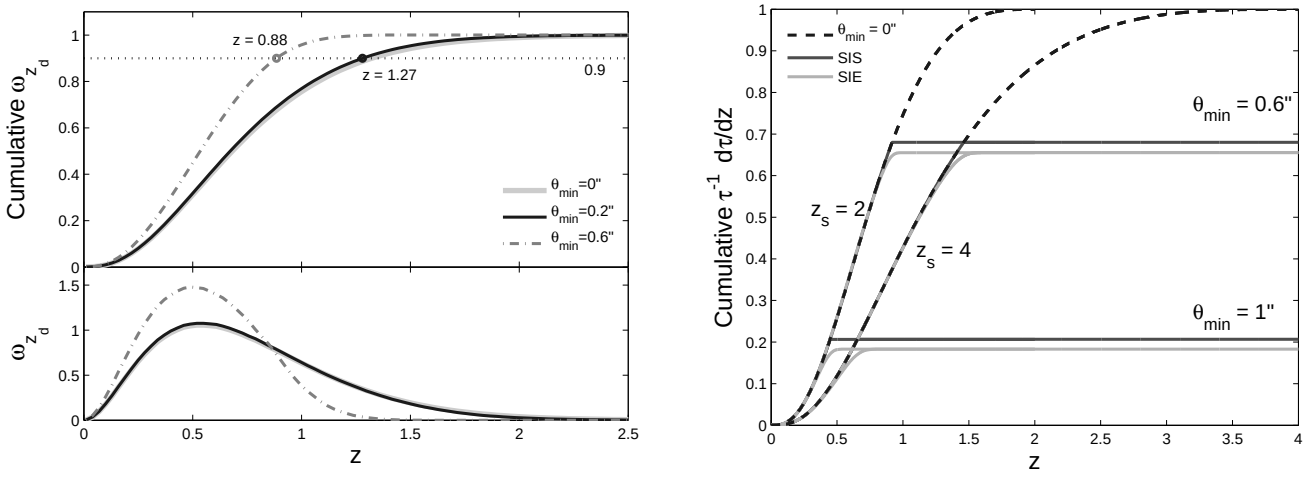

Fig. 6. *Left :*Normalised redshift distribution of the deflectors $\omega_{z_d}(z)$ and its cumulative representation, for three different values of the angular resolution $\theta_{min} = 0, 0.2$ and 0.6". *Right :* cumulative distribution $\tau^{-1} d\tau/dz$ as a function of the lens redshift.We show the case for two different source redshifts ($z_s = 2$ and 4) and three different values of the angular resolution parameter ($\theta_{min} = 0, 0.6$ and 1"), modeling the deflectors by means of the SIS and SIE models.

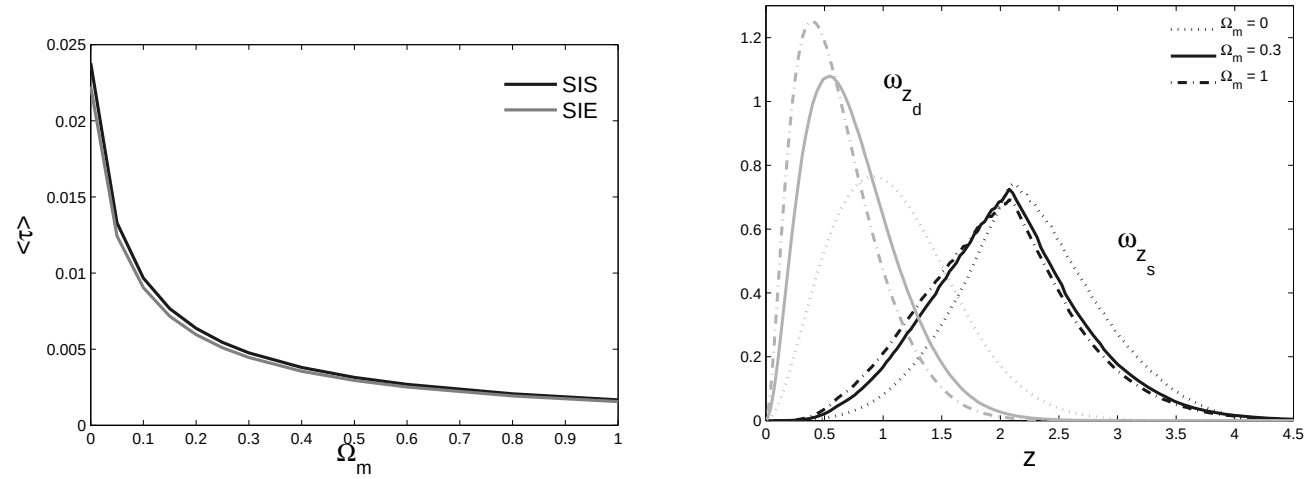

Fig. 7. *Left:* average optical depth $\langle\tau\rangle$ (considering all deflector types) as a function of the cosmological matter density parameter Ω_m, modeling the deflectors with the SIS and SIE models. *Right:* normalised redshift distributions ω_{z_s} and ω_{z_d} of the lensed sources and of the deflectors (for the early-type galaxy population), for different values of $\Omega_m = 0, 0.3$ and 1. All simulations were produced for the case $\theta_{min} = 0.2$".

density parameter Ω_m, assuming a flat FLRW universe, and considering the finite angular resolution $\theta_{min} = 0.2$" corresponding to the Gaia survey. We observe a very high dependence of the average optical depth as a function of Ω_m with an order of magnitude difference between the case of an empty universe and a universe full of matter ($\Omega_m = 0$ and 1, respectively). For this reason, using the fraction of lensed sources in a sample of sources has been proposed by Turner et al. (1984) to constrain the value of Ω_m.

There is a very good agreement between the observed behaviour when modeling the deflectors by means of the SIS and SIE deflectors, although, the SIS model always leads to a slight overestimate of the lensing optical depth.

In our simulations for the case of the SIE deflector, we have observed no dependence as a function of Ω_m of the relative fraction of lensing events with a given number of lensed images.

On the right panel of Fig. 7, we show the expected normalised redshift distribution of the lensed sources $\omega_{z_s}(z_s)$ and of the deflectors $\omega_{z_d}(z_d)$, for the three different values of $\Omega_m = 0, 0.3$ and 1. For the sake of clarity, we have only shown the deflector redshift distribution corresponding to the early-type galaxy population, but the one associated with the late-type population presents a similar behaviour. As previously mentioned, the normalised redshift distributions ω_{z_s} and ω_{z_d} obtained are identical for the SIS and SIE models. In order to minimise the computing time, we present the distributions obtained for the SIS model case.

Finally, in Fig. 8 we have represented the normalised distribution ω_{θ_E} as a function of the Einstein angle θ_E of the lensed sources, for different values of Ω_m. These distributions were obtained with the help of Eq. 23. We have considered the deflectors to be modeled with SIS deflectors and an angular resolution $\theta_{min} = 0.2$" corresponding to the Gaia survey. We find a very small dependence of $\omega_{\theta_E}(\theta_E)$ with the cosmological model parameter value.

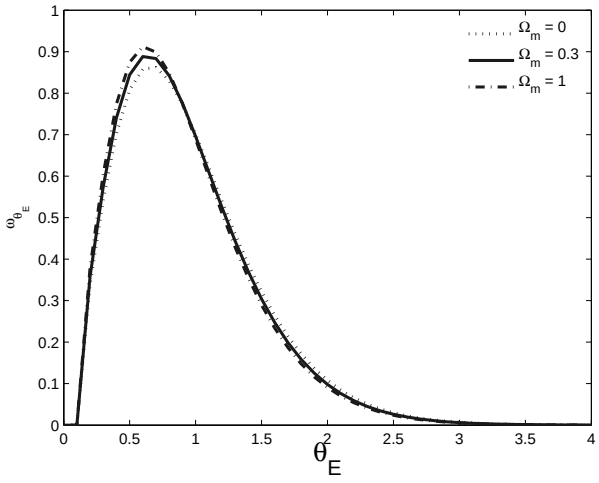

Fig. 8. Impact of the cosmological matter density parameter Ω_m on the normalised Einstein angular radius distribution $\omega_{\theta_E}(\theta_E)$ of the lensed sources. We have considered the deflectors to be modeled by SIS deflectors and an angular resolution $\theta_{min} = 0.2$" corresponding to the Gaia survey. θ_E is expressed in arcsecond.

We have also computed the normalised distribution $\omega_m(m)$ as a function of the apparent magnitude m and found no impact of Ω_m.

5. Conclusions

Out of the 6.64×10^5 QSOs brighter than $G = 20$ to be detected in the Gaia Survey, we expect the discovery of about 2886 multiply imaged sources, 450 of these being produced by a late-type galaxy . We have modeled the deflector population by means of the SIE and SIS mass distributions and found both model predictions to be in very good agreement, although the SIS model overestimates the mean lensing optical depth by $\sim 10\%$. Most of the multiply imaged sources will be composed of 2 images but we expect the detection of more than 250 lensed sources with more than 2 lensed images detected.

Among the lensed sources detected in the survey, we only expect ~ 1600 of these multiply imaged quasars to have an angular separation between their images large enough to be resolved from seeing limited observations (i.e. considering a ground-based survey without an adaptive optics system), allowing the acquisition of ground-based data to complement the spectra and time series provided by the satellite, ~ 80 of them having more than 2 lensed images detected.

We have shown that lenses with a deflector at high redshift tend to be missed as the angular resolution of a survey worsens, as these events are characterised by a smaller Einstein angular radius. Thanks to its angular resolution of $\theta_{min} = 0.2$", the lensed sources discovered in the Gaia survey will thus provide a unique statistical sample of lensed sources to study the evolution effects of the deflecting galaxy population, with the detection of ~ 800 lenses at a redshift between 0.8 and 2.

In this work, we have not considered the influence of the deflector environment which may produce an additional shear and convergence to the gravitational potential. Oguri et al. (2005) have shown that the additional convergence produced by the galaxy environment may increase the lensing probability (especially at large angular separation) by a boost of the image separation and amplification bias, mainly driven by convergence. Huterer et al. (2005) showed that the external shear increases the fraction of quads in a sample of lensed sources. The estimation in the present work of the number of lenses to be discovered by Gaia may thus slightly underestimate the lenses and quads to be discovered. We have also neglected the case of multiple deflectors at different redhshifts, as the probability for such an event would be of the order of $\langle\tau\rangle^2 \sim 10^{-5}$ which is negligeable compared to the lensing probability by a single deflector.

We have computed the normalised redshift distributions of the lensed sources ω_{z_s} and of the deflectors ω_{z_d} and found that these normalised distributions are the same whether modeling the deflectors by means of the SIS or the SIE mass distributions. The normalised deflector redshift distribution expected for the late-type galaxy population peaks at a higher redshift than that for the early-type one.

Furthermore, ω_{z_s} is independent of the angular resolution of the survey. As a consequence, we have concluded that the fraction of the optical depth lost by a source when increasing θ_{min} is independent of the redshift of the source.

Finally, we have analysed the impact of the cosmological matter density parameter Ω_m on the average lensing optical depth, as well as on the distributions as a function of the redshift of the lensed sources and deflectors. We conclude that all three are sensitive to the cosmological model parameter value and may be used to constrain the cosmological model. We have found no impact of Ω_m on the fraction of lensed sources as a function of the number of lensed images, as well as on the apparent magnitude distribution of the lensed sources.

References

Browne, I. W. A., Wilkinson, P. N., Jackson, N. J. F., et al. 2003, MNRAS, 341, 13
Chae, K.-H. 2010, Monthly Notices of the Royal Astronomical Society, 402, 2031
Choi, Y.-Y., Park, C., & Vogeley, M. S. 2007, The Astrophysical Journal, 658, 884
Finet, F., Elyiv, A., & Surdej, J. 2012, Memorie della Societa Astronomica Italiana, 83, 944
Harrison, D. L. 2011, Experimental Astronomy, 31, 157
Huterer, D., Keeton, C. R., & Ma, C.-P. 2005, ApJ, 624, 34
Inada, N., Oguri, M., Shin, M.-S., et al. 2012, AJ, 143, 119
Jordi, C., Gebran, M., Carrasco, J. M., et al. 2010, A&A, 523, A48
Jordi, C., Høg, E., Brown, A. G. A., et al. 2006, MNRAS, 367, 290
Keeton, C. R., Kochanek, C. S., & Falco, E. E. 1998, ApJ, 509, 561
Kochanek, C. S., Falco, E. E., Impey, C. D., et al. 2000, ApJ, 543, 131
Koopmans, L. V. E., Bolton, A., Treu, T., et al. 2009, ApJ, 703, L51
Koopmans, L. V. E., Treu, T., Bolton, A. S., Burles, S., & Moustakas, L. A. 2006, The Astrophysical Journal, 649, 599
Kormann, R., Schneider, P., & Bartelmann, M. 1994, Astronomy and Astrophysics, 284, 285
Mignard, F. 2005, 576, 5
Mignard, F. 2008, in Gaia - SIM
Mignard, F. 2012, Mem. Soc. Astron. Italiana, 83, 918
Mitchell, J. L., Keeton, C. R., Frieman, J. A., & Sheth, R. K. 2005, ApJ, 622, 81
Nemiroff, R. J. 1989, ApJ, 341, 579
Oguri, M., Inada, N., Strauss, M. A., et al. 2012, AJ, 143, 120
Oguri, M., Keeton, C. R., & Dalal, N. 2005, MNRAS, 364, 1451
Oguri, M. & Marshall, P. J. 2010, MNRAS, 405, 2579
Palanque-Delabrouille, N., Magneville, C., Yèche, C., et al. 2013, A&A, 551, A29
Peebles, P. 1993, Principles of Physical Cosmology, ed. P. S. in Physics (Princeton University Press)
Richards, G. T., Croom, S. M., Anderson, S. F., et al. 2005, MNRAS, 360, 839
Richards, G. T., Strauss, M. A., Fan, X., et al. 2006, The Astronomical Journal, Volume 131, Issue 6, pp. 2766-2787, Volume 131, Issue 6, 2766
Robin, A. C., Luri, X., Reylé, C., et al. 2012, A&A, 543, A100
Ross, N. P., McGreer, I. D., White, M., et al. 2012, ArXiv e-prints
Schneider, P., Ehlers, J., & Falco, E. E. 1992, Gravitational Lenses
Shen, Y. & Kelly, B. C. 2012, ApJ, 746, 169

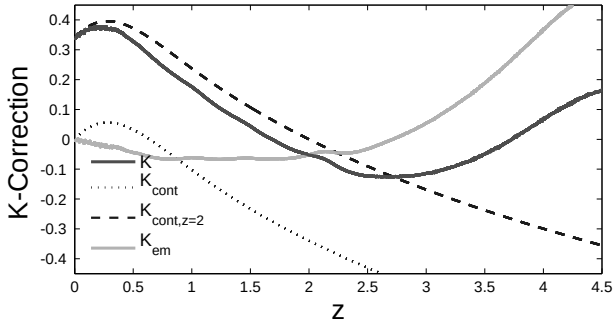

Fig. A.1. K-Correction in the Gaia photometric G-band as a function of the redshift. We have represented the total K-Correction (K) with zero point of the continuum contribution at $z = 2$, the continuum contributions with zero points at $z = 0$ and $z = 2$ (K_{cont} and $K_{cont,z=2}$), and the emission line contribution (K_{em}).

Sheth, R. K., Bernardi, M., Schechter, P. L., et al. 2003, The Astrophysical Journal, 594, 225
Slezak, E. & Mignard, F. 2007, Technical Report, Observatoire de la Côte d'Azur, GAIA-C2-TN-OCA-ES- 001-1
Sluse, D., Chantry, V., Magain, P., Courbin, F., & Meylan, G. 2012, Astronomy & Astrophysics, 538, A99
Turner, E. L., Ostriker, J. P., & Gott, J. R. 1984, Astrophysical Journal, 284, 1
Vanden Berk, D. E., Richards, G. T., Bauer, A., et al. 2001, The Astronomical Journal, Volume 122, pp. 549

Appendix A: Gaia G-band K-correction and magnitude conversion

We here describe the different relations used to convert absolute magnitudes between the Gaia and the SDSS photometric systems.

We follow Richards et al. (2006) and express the absolute magnitudes M in the Gaia G-band as magnitudes of the continuum, with a zero point of the continuum K-correction at redshift $z = 2$. M is thus defined by

$$M = m - DM - K_{em} - K_{cont,z=2}, \tag{A.1}$$

where K_{em} is the contribution due to the emission lines and $K_{cont,z=2}$ the continuum K-Correction with zero point at redshift $z = 2$.

To estimate the K-correction of the Gaia photometric G-band, we have computed the correlation between the G-band spectral transmission function (in terms of wavelengths) with the QSO synthetic spectrum derived from SDSS QSO spectra by Vanden Berk et al. (2001). The synthetic spectrum ranging from 3800 to 9200 Å could not cover the entire wavelength range of the G filter (3210 – 11020 Å in the observer comoving reference frame). As the synthetic spectrum was well fitted by a continuum spectrum with spectral index $\alpha_\nu = -0.46$ between the Ly-α and Hβ lines, and $\alpha_\nu = -1.58$ for wavelengths longer than the Hβ line (Vanden Berk et al. 2001), we have extrapolated the synthetic spectrum towards longer wavelengths assuming a continuum spectrum with spectral index $\alpha_\nu = -1.58$.

We have computed the contribution of the continuum to the K-correction assuming a break in the spectral index, considering the zero points of the K-Correction at $z = 0$ and $z = 2$, K_{cont} and $K_{cont,z=2}$, respectively. The behaviour of $K_{cont,z=2}$ as a function of the redshift are displayed in Fig. A.1.

Finally, the contribution to the apparent magnitude of the emission lines K_{em}, is given by $K_{em} = K - K_{cont,z=2}$. The computed K-correction is shown as a function of the redshift in Fig. A.1.

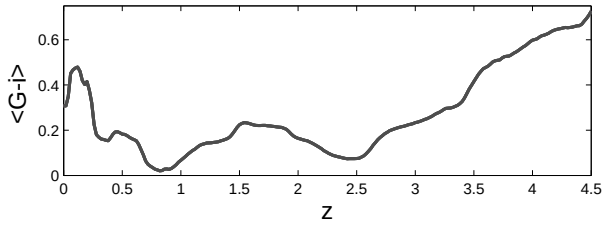

Fig. A.2. Average colour transformation $\langle G - i \rangle (z)$ as a function of the QSO redshift, assuming the source spectral type to be that of Vanden Berk et al. 2001 and both magnitude systems to be AB-magnitudes.

In order to convert the absolute magnitudes M_i from the SDSS i-band to the Gaia G-band absolute magnitude M, we used the K-correction for the SDSS i-band given in Richards et al. (2006), the G-band K-correction previously described and we have calculated an average apparent magnitude transformation between the Gaia G-magnitude and SDSS-i magnitude as follows

$$\langle G - i \rangle (z) = -2.5 \log \left[\frac{\int S(\lambda (1+z)) T_G(\lambda) d\lambda}{\int S(\lambda (1+z)) T_i(\lambda) d\lambda} \right] + 2.5 \log \left[\frac{\int \lambda^{-2} T_G(\lambda) d\lambda}{\int \lambda^{-2} T_i(\lambda) d\lambda} \right] \tag{A.2}$$

where $S(\lambda)$ is the synthetic QSO spectrum from Vanden Berk et al. (2001), $T_G(\lambda)$ and $T_i(\lambda)$ are the spectral transmission of the G and i bands, considering both magnitudes in the AB-magnitude system. The behaviour of $\langle G - i \rangle (z)$ as a function of the redshift is shown in Fig. A.2.

The absolute magnitude average transformation is given by

$$M = M_i + K_i(z) - K(z) + \langle G - i \rangle (z). \tag{A.3}$$

where $K(z)$ and $K_i(z)$ are the K-corrections in the G-band and SDSS i-band, respectively.

Appendix B: ω_{z_d} dependence on the deflector type

In this appendix, we demonstrate that ω_{z_d} is independent of the deflector type under the assumption of constant deflector comoving density and a perfect instrument. For simplicity, we consider the case of deflectors modeled by an SIS mass distribution.

The expression of τ_{SIS} in Eq. 8 can be further developed by inserting the expression of $\Sigma_* = \Sigma_{SIS}(\sigma_*)$ which, using the definition of θ_E in Eq. 2 and that of Σ_{SIS} in Eq. 3, may be written as

$$\Sigma_* = \left(\frac{4\pi\sigma_*^2}{c^2} \right)^2 \left(\frac{D_{od} D_{ds}}{D_{os}} \right)^2 \iint_{S_y} B(m, \mathbf{y}) \, d\mathbf{y}. \tag{B.1}$$

Inserting the latter expression into Eq. 8 leads to

$$\tau_{SIS}(z_s, m) = \left(\left(\frac{4\pi\sigma_*^2}{c^2} \right)^2 \beta \Phi_* \frac{\Gamma((\alpha+4)/\beta)}{\Gamma(\alpha/\beta)} \right) \int_0^{z_s} \zeta(z, z_s) \iint_{S_y} B(m, \mathbf{y}) \, d\mathbf{y} dz, \tag{B.2}$$

where we have defined $\zeta(z, z_s) = (1+z)^3 \frac{cdt}{dz} (D_{od} D_{ds})^2 / D_{os}^2$. The coefficient in brackets includes all the dependence to the

parameters describing the VDFs ($\Phi_*, \sigma_*, \alpha, \beta$), which may refer to either the early- or late-type galaxies. In our development, the deflector comoving density is assumed constant therefore the VDF parameters do not depend on the redshift.

We may obtain an expression for $\frac{d\tau}{dz}(z_s, z_d, M)$ differentiating the former expression of τ_{SIS} with respect to the deflector redshift z. The result is

$$\frac{d\tau}{dz}(z_s, z_d, M) = \left(\left(\frac{4\pi\sigma_*^2}{c^2}\right)^2 \beta\Phi_* \frac{\Gamma\left(\left(\alpha+4\right)/\beta\right)}{\Gamma\left(\alpha/\beta\right)}\right) \zeta(z, z_s) \iint_{S_y} B(m, \mathbf{y})\, d\mathbf{y}. \quad \text{(B.3)}$$

For a perfect instrument, τ_{SIS} and $\frac{d\tau}{dz}$ have an identical dependence on the VDF parameters, shown in the first factor of Eqs. B.2 and B.3. Therefore, when calculating the normalised redshift distribution of the deflectors by inserting Eqs. B.2 and B.3 into the definition of ω_{z_d} (Eq. 18) and using the definition of $\langle\tau\rangle$ (Eq. 16), the factors containing the VDF parameters cancel each other, as long as we assume no redshift or absolute magnitude dependence of the VDF parameters. For a perfect instrument, ω_{z_d} is thus identical for early- and late-type galaxy deflectors as it does no longer depend on the parameters defining the deflector VDF (Φ_*, σ_*, α and β).

However, when the finite angular resolution of the survey is taken into account, the integration area for the lensing cross section S_y is now a function of the ratio θ_{min}/θ_*, with $\theta_* \propto \sigma_*^2$. This dependence in σ_* leads to different results for the two deflector types as this parameter differs for the early- and late-type galaxy VDF.